

**DIGITAL HOLOGRAPHIC INTERFEROMETRY
FOR THE MEASUREMENT OF TEMPERATURE
PROFILE, HEAT DISSIPATION AND
CONTOURING**

VARUN KUMAR



INSTRUMENT DESIGN DEVELOPMENT CENTRE

INDIAN INSTITUTE OF TECHNOLOGY DELHI

NEW DELHI – 110016, INDIA

SEPTEMBER 2016

© Indian Institute of Technology Delhi (IITD), New Delhi, 2016

**DIGITAL HOLOGRAPHIC INTERFEROMETRY
FOR THE MEASUREMENT OF TEMPERATURE
PROFILE, HEAT DISSIPATION AND
CONTOURING**

by

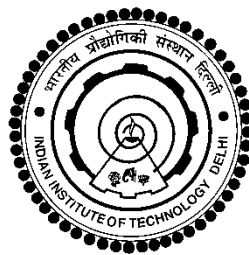
VARUN KUMAR

INSTRUMENT DESIGN DEVELOPMENT CENTRE

Submitted

in fulfillment of the requirements of the degree of Doctor of Philosophy

to the



**INDIAN INSTITUTE OF TECHNOLOGY DELHI
SEPTEMBER 2016**

DEDICATED TO
MY
PARENTS

CERTIFICATE

This is to certify that the thesis entitled “**DIGITAL HOLOGRAPHIC INTERFEROMETRY FOR THE MEASUREMENT OF TEMPERATURE PROFILE, HEAT DISSIPATION AND CONTOURING**” being submitted by **Mr. VARUN KUMAR** to the Indian Institute of Technology Delhi for the award of the degree of “**DOCTOR OF PHILOSOPHY**”, is a record of the authentic research work carried out by him under my supervision and guidance. He has fulfilled all the requirements for submission of this thesis, which to the best of my knowledge has reached the required standard.

The material contained in this thesis has not been submitted in part or full to any other University or Institute for the award of any other degree.

Dr. Chandra Shakher
Professor
Instrument Design Development Centre
Indian Institute of Technology Delhi
Hauz Khas – 110016, New Delhi, India

ACKNOWLEDGEMENTS

First and foremost, I am sincerely thankful to my supervisor **Prof. Chandra Shakher** for his constant encouragement, guidance and never-ending patience. It was an honor and privilege to learn the insight of methodology of research and experimentation from him. Credit of introducing me to the area of digital holography goes to him. The joy and enthusiasm he has for his research was contagious and motivational for me, even during tough times in my Ph.D. The thesis could have never been successful without his insightful suggestions, ungrudging support and timely guidance. I also, express my profound indebtedness to him not only for the time he took out from his hectic schedule to guide me during the course of the thesis but also for the help he provided me to get international exposures via conferences and interaction with scientists working in the field of holography. He would have never accepted anything less than my best efforts, and for that, I thank him.

I am highly grateful to all my student research committee members **Prof. A. L. Vyas, Prof. M. R. Shenoy, Prof. D. S. Mehta** and **Dr. Gufran S. Khan** for providing technical advice, constant encouragement and inspiration.

I am also very thankful to **Dr. Md. Mosarraf Hossain, Dr. Gyanendra Sheoran** and **Dr. Shobhna Sharma** who has been with me during the initial stage of research work in the Laser Applications and Holography Laboratory. I would like to give my heartfelt thanks to them for always encouraging me to do better in my thesis work. They are the first person, to help me in my initial experimentation.

I would like to express my deepest thanks and acknowledgement with gratitude and affection to **Mr. Manoj Kumar, Ms. Shilpi Agarwal, Dr. Vishal Srivastava, Dr. Md. Inam, Mr. Kanchan Kumar Agarwal, Mr. Divya Kumar, Ms. Sruthi Prasood, and Mr. Pranav Kumar Pandey**, who helped me in many ways at different stages of my thesis work in the Laser Applications and Holography Laboratory, Indian Institute of Technology, Delhi.

Thanks are also due to the technical staff, particularly, **Mr. Rajaram, Mr. Surinder Singh** and **Mr. S. C. Bansal**, of the workshop in Instrument Design Development Centre for extending their valuable help at times.

The equipment used in the experiment which was purchased from Department of Science and Technology (DST), Govt. of India project and Defence Research and Development Organization (DRDO), Ministry of Defence, Govt. of India project is greatly acknowledged.

I express deep sense of gratitude to my parents, who raised me with love of science and supported me in all my pursuits. I am also thankful to my brother for his love, support encouragement and faith in me. Last but not the least, I am grateful to my family members and friends whose support and inspiration in various stages of my research work in the laboratory have greatly helped me to realize the thesis work.

Date:

Varun Kumar

ABSTRACT

Optical interferometric techniques are widely used for scientific and industrial measurements. These techniques have become more powerful after the development of laser and holography. Holography added new dimension to the interferometry and made it a more powerful and useful tool for its applications in industries. Developments in electronic imaging devices and high speed computers have provided more flexibility in recording and reconstruction of holograms in comparison of recording on high resolution recording material for measurement purpose. Recording of holograms by digital imaging devices and reconstruction by numerical methods is termed as digital holography (DH). This has made possible the quantitative measurement of amplitude and phase of an object wavefront from a single recorded digital hologram. By using digital holography interference phase between two states of object wavefronts can be directly calculated from two digital holograms by subtracting the numerically evaluated phases in two different states of the object without using phase shifting interferometry. Thus, digital holographic interferometry (DHI) avoids extra efforts to calculate the interference phase. This provides the flexibility in the measurement and makes the process of measurement faster, robust and almost real time.

The thesis is organized in six chapters.

Chapter I provide the brief introduction of conventional holography and digital holography. This chapter provides the detailed description of digital hologram recording process and different techniques for numerical reconstruction of holograms and its application in metrology. This chapter also provides the brief outlines of the research work presented in this thesis.

Chapter II describes the measurement of natural local convective heat transfer coefficient (h_c) along the surface of electrically heated tungsten wires of different diameters and different heating conditions of wire placed in vertical position using lensless Fourier transform digital holographic interferometry (LLFTDHI).

Chapter III presents the investigations about the heat dissipation process of plate fin heat sink using LLFTDHI under different heating conditions and the effect of fin spacing on the heat dissipation performance of heat sink is also investigated. These investigations may help to make proper choice of heat sink in electronic circuit.

Chapter IV describes a method for contouring of diffused objects using digital holographic moiré interferometry (DHMI) in lensless Fourier transform configuration. Fringe projection moiré technique combined with digital double-exposure holography produces the contours in this method. This method may find important application for shape measurement.

Chapter V deals with a method for the testing (lens height profile, sag height and radius of curvature) of refractive micro-lens using Mach-Zehnder based digital holographic interferometric microscope (DHIM). Height profile of micro-lenses measured by DHIM is compared with Coherence Correlation Interferometer (CCI) from Taylor Hobson Ltd. UK with axial resolution 0.1 A^0 . Root mean square deviation between the measurement done by DHIM and CCI is 0.12%.

In Chapter VI holo-shear lens made on dichromated gelatin (DCG) is used as a lateral shear interferometer for the measurement of temperature profile inside the candle flame. Results are encouraging.

CONTENTS

| | |
|---|-------------|
| <i>CERTIFICATE</i> | i |
| <i>ACKNOWLEDGEMENTS</i> | ii |
| <i>ABSTRACT</i> | iv |
| <i>CONTENTS</i> | vi |
| <i>LIST OF FIGURES</i> | x |
| <i>LIST OF TABLES</i> | xvi |
| <i>LIST OF SYMBOLS</i> | xvii |
| CHAPTER 1: INTRODUCTION | 1-33 |
| 1.1 Holography | 1 |
| 1.2 Digital Holography: Development History | 5 |
| 1.2.1 Recording of Digital Holograms | 10 |
| 1.2.2 Numerical Reconstruction of Holograms | 13 |
| 1.3 Some Widely used Numerical Reconstruction Methods | 16 |
| 1.3.1 Fresnel Reconstruction Method | 16 |
| 1.3.2 Convolution Method | 19 |
| 1.3.3 Angular Spectrum Method | 21 |
| 1.3.4 Phase-Shifting Method | 23 |
| 1.3.5 Lens-Less Fourier Transform Digital Holography | 24 |
| 1.3.6 Discussion | 29 |
| 1.4 Digital Holographic Interferometry and its Applications | 31 |

| | | |
|-------------------|---|--------------|
| 1.5 | Outlines of the Research Work Done in the thesis | 33 |
| CHAPTER 2: | MEASUREMENT OF NATURAL CONVECTIVE | 34-59 |
| | HEAT TRANSFER COEFFICIENT ALONG THE SURFACE | |
| | OF HEATED WIRE USING DIGITAL HOLOGRAPHIC | |
| | INTERFEROMETRY | |
| 2.1 | Introduction | 34 |
| 2.2 | Theory | 40 |
| | 2.2.1 Conversion of Integral form to Discrete form | 42 |
| | 2.2.2 Measurement of Temperature and Convective Heat Transfer Coefficient | 45 |
| 2.3 | Experimental | 46 |
| 2.4 | Results and Discussion | 51 |
| | 2.4.1 Experiment for Three Different Heating Conditions of Wire | 51 |
| | 2.4.2 Experiment on Wires of Three Different Diameters of Equal Length with a Constant Power applied Across Wire | 56 |
| 2.5 | Conclusion | 59 |
| CHAPTER 3: | STUDY OF HEAT DISSIPATION PROCESS FROM HEAT | |
| | SINK USING LENSLESS FOURIER TRANSFORM DIGITAL | 60-80 |
| | HOLOGRAPHIC INTERFEROMETRY | |
| 3.1 | Introduction | 60 |
| 3.2 | Theory | 64 |
| 3.3 | Experimental | 66 |
| 3.4 | Results and Discussion | 69 |
| 3.5 | Conclusion | 80 |

| | |
|---|----------------|
| CHAPTER 4: CONTOURING OF DIFFUSED OBJECTS USING | 81-98 |
| LENSLESS FOURIER TRANSFORM DIGITAL MOIRÉ | |
| HOLOGRAPHY | |
| 4.1 Introduction | 81 |
| 4.2 Theory: Contouring Methodology | 86 |
| 4.3 Experimental | 88 |
| 4.4 Numerical Processing of Digital Holograms | 90 |
| 4.5 Results and Discussion | 92 |
| 4.6 Conclusion | 98 |
| CHAPTER 5: TESTING OF MICRO-OPTICS USING DIGITAL | 99-111 |
| HOLOGRAPHIC INTERFEROMETRIC MICROSCOPY | |
| 5.1 Introduction | 99 |
| 5.2 Experimental | 101 |
| 5.3 Hologram Reconstruction | 103 |
| 5.4 Results and Discussion | 105 |
| 5.4.1 Reconstruction of USAF Resolution Test Chart | 105 |
| 5.4.2 Results of Testing of Micro-lenslet Array | 107 |
| 5.5 Conclusion | 111 |
| CHAPTER 6: MEASUREMENT OF TEMPERATURE AND | 112-127 |
| TEMPERATURE PROFILE OF CANDLE FLAME USING | |
| HOLO-SHEAR LENS AND FOURIER FRINGE | |
| ANALYSIS TECHNIQUE | |
| 6.1 Introduction | 112 |
| 6.2 Theory | 114 |
| 6.2.1 Recording of Holo-Shear lens | 114 |

| | |
|--|---------|
| 6.2.2 Lateral Shearing Interferometry | 117 |
| 6.3 Experimental | 121 |
| 6.4 Results and Discussion | 123 |
| 6.5 Conclusion | 127 |
| CHAPTER 7: CONCLUSION | 128-130 |
| <i>FUTURE SCOPE OF THE WORK</i> | 131-132 |
| <i>REFERENCES</i> | 133-165 |
| <i>LIST OF PUBLICATIONS</i> | 166-167 |
| <i>AUTHOR'S BIOGRAPHY</i> | 168 |

LIST OF FIGURES

| | |
|-------------|---|
| Fig. 1.1(a) | Schematic of experimental set-up of off-axis hologram recording. |
| Fig. 1.1(b) | Schematic of off-axis hologram reconstruction geometry. |
| Fig. 1.2(a) | Schematic of off-axis digital holographic set-up for recording a hologram. |
| Fig. 1.2(b) | Geometry for recording a digital Fresnel hologram. |
| Fig. 1.3 | Schematic of Co-ordinate system used for recording and reconstruction of digital hologram. |
| Fig. 1.4(a) | Geometry showing the variation of angle between object wave and plane reference wave over the surface of sensor. |
| Fig. 1.4(b) | Geometry used in LLFTDHI for constant angle between object and spherical reference wave. |
| Fig. 1.5 | Schematic of experimental set-up for LLFTDH. |
| Fig. 1.6 | Procedure for the reconstruction of digital hologram. |
| Fig. 1.7(a) | Real image, virtual image and dc term of lord Buddha reconstructed using LLFTDH. |
| Fig. 1.7(b) | Real image after removal of virtual image and dc term. |
| Fig. 2.1(a) | Cross-section of an axisymmetric phase difference. |
| Fig.2.1(b) | Process of finding the area matrix. |
| Fig.2.1(c) | Illustration of Abel inversion by geometrical relationship. |
| Fig.2.2(a) | Schematic of experimental set-up for the measurement of convective heat transfer coefficient. |
| Fig. 2.2(b) | Photograph of mount to clamp the wire in vertical position. |
| Fig. 2.3 | Photograph of experimental set-up. |
| Fig. 2.4 | Flow chart for calculation of temperature and convective heat transfer coefficient from two digitally recorded holograms. |

| | |
|---|---|
| Fig. 2.5(a) | Phase difference maps of air without and with heating a wire of diameter 0.4 mm when the power applied across the wire is 70 W. |
| Fig. 2.5(b ₁ .b ₄) | Line profile of the phase difference maps along the lines AB, CD, EF, and GH, respectively, as marked in Fig. 2.5(a). |
| Fig. 2.5(c) | 3D phase difference map corresponding to Fig. 2.5(a) |
| Fig. 2.5(d) | Refractive index difference distribution along the lines AB, CD, EF, and GH as marked in Fig. 2.5(a). |
| Fig. 2.5(e) | Temperature profile of heated air along the lines AB, CD, EF, and GH as marked in Fig. 2.5(a). |
| Fig. 2.6(a) | Phase difference map of air without and with heating wire when applied power across the wire is 46.8 W. |
| Fig. 2.6(b) | 3D phase difference map corresponding to Fig. 2.6 (a). |
| Fig. 2.6(c) | Temperature profile along the line AB, CD, EF and GH as marked in Fig. 2.6 (a). |
| Fig. 2.7(a) | Phase difference map of air without and with heating wire when applied power across the wire is 37 W. |
| Fig. 2.7(b) | 3D phase difference map corresponding to Fig. 2.7(a). |
| Fig. 2.7(c) | Temperature profile along the line AB, CD, EF and GH as marked in Fig.2.7(a). |
| Fig. 2.7(d) | Comparison between temperature profile measured by DHI and thermocouple |
| Fig. 2.8(a) | Phase difference map of ambient air and heated air around a wire of diameter 0.6 mm when the power applied across the wire is 70 W. |
| Fig. 2.8(b) | 3D phase difference map corresponding to Fig. 2.8(a). |
| Fig. 2.8(c) | Temperature profile of heated air along the lines AB, CD, EF, and GH as marked in Fig. 2.8(a). |
| Fig. 2.9(a) | Phase difference map of ambient air and heated air around a wire of diameter 0.78mm when the power applied across the wire is 70 W. |
| Fig. 2.9(b) | 3D phase difference map corresponding to Fig. 2.9(a). |
| Fig. 2.9(c) | Temperature profile of heated air along the lines AB, CD, EF, and GH as |

| | |
|---------------|---|
| | marked in Fig. 2.9(a). |
| Fig. 3.1(a) | Schematic of LLFT configuration of Digital holographic set-up to study the heat dissipation process from heat sink. |
| Fig. 3.1(b) | Photograph of heat sink used in the experiment. |
| Fig. 3.1(c) | Photograph of experimental set-up to study heat dissipation process from aluminum plate fin heat sink using LLFTDH. |
| Fig. 3.2(a) | Phase difference map of air field surrounding heat sink in steady state. |
| Fig. 3.2(b) | Line profile of wrapped phase difference map of air along line AB in vertical direction as shown in Fig. 3.2(a). |
| Fig. 3.2(c) | Unwrapped phase difference map corresponding to Fig. 3.2(a). |
| Fig. 3.2(d) | Unwrapped phase difference profile corresponding to Fig. 3.2(b). |
| Fig. 3.2(e) | 2D temperature distribution of heated air corresponding to Fig. 3.2(a). |
| Fig. 3.2(f) | Temperature profile along line AB as marked on Fig. 3.2(a). |
| Fig. 3.3(a-h) | Reconstructed wrapped phase difference maps of air surrounding the heat sink at different times during heating process. |
| Fig. 3.4 | Temperature profile at different time along line AB in vertical direction corresponding to Fig. 3.3(a-g). |
| Fig. 3.5 | Reconstructed wrapped phase difference map of heated air surrounding heat sink in steady state when applied power across the load resistor was 16.8 W. |
| Fig. 3.6 | Reconstructed temperature profile along horizontal lines ab, cd, ef, and gh starting from the top of fins of heat sink in vertical direction corresponding to Fig. 3.5. |
| Fig. 3.7(a) | Reconstructed wrapped phase difference map of air field when 7.6 W power was applied to the load resistor. |
| Fig. 3.7(b) | Reconstructed wrapped phase difference map of air field when 12 W power was applied to the load resistor. |
| Fig. 3.7(c) | Reconstructed wrapped phase difference map of air field when 16.8 W power was applied to the load resistor. |

| | |
|---|--|
| Fig. 3.8 | Reconstructed temperature profile of air field along line AB corresponding to Figs. 3.7(a-c) in three heating conditions of load resistor connected to heat sink. |
| Fig. 3.9 | Reconstructed wrapped phase difference map of air field when (a) $S_1= 3.25$ mm; (b) $S_2 = 5$ mm; and (c) $S_3=9$ mm. |
| Fig. 3.10 | Reconstructed temperature distribution with channel width (a) $S_1= 3.25$ mm; (b) $S_2= 5$ mm; and (c) $S_3= 9$ mm. |
| Fig. 3.11 | Temperature profile along the line AB corresponding to Figs. 3.9(a-c). |
| Fig. 4.1 | Schematic of the geometry for moiré fringe formation. |
| Fig. 4.2(a) | Schematic of set-up for digital holographic moiré contouring. |
| Fig. 4.2(b) | Photograph of experimental set-up for contouring of diffused object using lensless Fourier transform digital moiré holography. |
| Fig. 4.3 | Flow chart of formation of modified grid, reference grid and moiré contour fringes. |
| Fig. 4.4 | Reconstructed primary image of the cube. |
| Fig. 4.5(a ₁) | Modified grid reconstructed from two digital holograms; first digital hologram $H_1(\beta)$ recorded with initial object illumination angle ($\beta = 41^\circ$) and second hologram $H_2(\beta-\theta)$ recorded with a tilt ($\theta=0.0025^\circ$) about initial object illumination angle $\beta = 41^\circ$. |
| Fig. 4.5(b ₁) | Reference grid reconstructed from second digital hologram $H_2(\beta-\theta)$ and third digital hologram $H_3(\beta-\theta, 2t)$ recorded with final object illumination angle ($\beta-\theta$) unchanged and detector translation $2t= 0.15$ mm. |
| Fig. 4.5(c ₁) | Moiré contour fringes reconstructed from first hologram $H_1(\beta)$ and third hologram $H_3(\beta-\theta, 2t)$. |
| Fig. 4.5(a ₂ -c ₂) | Modified grid, reference grid, and the moiré contour fringes corresponding to tilt in object illumination beam ($\theta= 0.005^\circ$) and detector translation $2t = 0.15$ mm. |
| Fig. 4.6(a ₁ .a ₅) | Moiré contour fringes corresponding to mirror rotation and detector translation pairs of, respectively, ($0.0067^\circ, 0.20$ mm), ($0.01^\circ, 0.25$ mm), |

| | |
|-------------|---|
| | (0.0067° , 0.30 mm), (0.01° , 0.50 mm), and (0.015° , 0.70 mm). |
| Fig. 5.1(a) | Schematic of Mach-Zehnder interferometer based digital holographic interferometric microscope for testing of micro-lens array. |
| Fig. 5.1(b) | Photograph of DHIM experimental set-up used for the testing of refractive micro-lens array. |
| Fig. 5.2(a) | Hologram of USAF resolution chart. |
| Fig. 5.2(b) | Fourier spectrum of hologram. |
| Fig. 5.2(c) | Intensity image. |
| Fig. 5.3 | Flow chart of calculation of height map of micro-lenslet array. |
| Fig. 5.4(a) | Modulo 2π phase difference map of micro-lens array and ambient air. |
| Fig. 5.4(b) | 2D unwrapped phase difference map of micro-lens array and ambient air. |
| Fig. 5.4(c) | 3D unwrapped phase difference map of micro-lens array and ambient air. |
| Fig. 5.5(a) | 3D height map of micro-lens array. |
| Fig. 5.5(b) | Height profile of micro-lenses along the line AB as marked in Fig. 5.4(b). |
| Fig. 5.6 | Comparison of height profiles of micro-lenses array obtained by digital holographic interferometric microscopy (DHIM) and Coherence Correlation Interferometer. |
| Fig. 6.1 | Recording geometry of holo-shear lens. |
| Fig. 6.2 | Light ray passing through axi-symmetric temperature field. |
| Fig. 6.3(a) | Schematic of the experimental set-up of holo-shear interferometry for temperature measurement. |
| Fig. 6.3(b) | Photograph of experimental set-up for temperature measurement inside candle flame using holo-shear lens. |
| Fig. 6.4(a) | Recorded sheared interferogram of air (without flame) in +x direction. |
| Fig. 6.4(b) | Recorded sheared interferogram of flame in +x direction. |
| Fig. 6.5(a) | Wrapped phase map of air in absence of flame corresponding to Fig. 6.4(a). |

| | |
|-------------|--|
| Fig. 6.5(b) | Wrapped phase map of air in presence of flame corresponding to Fig. 6.4(b). |
| Fig. 6.6(a) | 3-D unwrapped phase map of air in absence of flame of selected portion from Fig. 6.5(a). |
| Fig. 6.6(b) | 3-D unwrapped phase map of air in presence of flame of selected portion from Fig. 6.5(b). |
| Fig. 6.7(a) | 3-D unwrapped phase difference map of air with and without the flame. |
| Fig. 6.7(b) | Unwrapped phase difference profile along the line AB as marked in Fig. 6.5(a) at height 10 mm from the base of candle flame. |
| Fig. 6.8(a) | Refractive index difference profile inside the candle flame at a height of 10 mm. |
| Fig. 6.8(b) | Temperature profile inside the candle flame at a height of 10 mm. |

LIST OF TABLES

- Table 2.1 Experimentally calculated values of local natural convective heat transfer coefficient for three heating conditions of wire
- Table 2.2 Calculated values of convective heat transfer coefficient (h_c) from digital holographic interferometry (DHI) for wires of three different diameters
- Table 3.1 Experimentally calculated values of base temperature, local heat flux and local convective heat transfer coefficient
- Table 3.2 Experimentally calculated values of local heat flux and local convective heat transfer coefficient for different channel widths of heat sink
- Table 4.1 The experimental and theoretical values of the modified and the reference grid periods as well as the moiré contour intervals corresponding to the seven different mirror rotation and detector translation pair

LIST OF SYMBOLS

| | |
|------------|--|
| X_O | X coordinate in object plane |
| Y_O | Y coordinate in object plane |
| X | X coordinate in hologram plane |
| Y | Y coordinate in hologram plane |
| X_I | X coordinate in image plane |
| Y_I | Y coordinate in image plane |
| $H(X,Y)$ | Intensity distribution of the interference pattern at hologram plane |
| O | Complex amplitude of the object wave |
| R | Complex amplitude of the reference wave |
| R^* | Complex conjugate of reference wave |
| O^* | Complex conjugate of object wave |
| $E_R(p,q)$ | Digital spherical reference wave |
| $H(p,q)$ | Digital hologram |
| $O(m,n)$ | Digital reconstructed object wavefront |
| d_f | Fringe spacing |
| d | Distance of object from the camera |
| d_0 | Maximum lateral extension of object |
| f_{max} | Maximum spatial frequency of CCD detector |

| | |
|-----------------|--|
| $I(m,n)$ | Digital reconstructed object intensity |
| ΔX | Sampling interval along X axis in the hologram plane/pixel size in x direction |
| ΔY | Sampling interval along Y axis in the hologram plane/pixel size in Y direction |
| ΔX_I | Sampling interval along X axis in the image plane |
| ΔY_I | Sampling interval along Y axis in the image plane |
| λ | Wavelength of the laser light |
| k | Wave vector |
| $M \times N$ | Number of pixels in the sensor |
| g | Impulse response of free space propagation |
| m, n | integers $m = 0,1,2,3,4,\dots,M$ $n = 0,1,2,3,4,\dots,N$ |
| FFT | Fast Fourier transform |
| Ψ_{TD} | Digital transmitted wave front |
| $R_D(p,q)$ | Digital Plane reference wave |
| $\phi(m,n)$ | Phase distribution of a reconstructed object wavefront |
| $IFFT$ | Inverse Fast Fourier transformation |
| d_1, d_2, d_3 | Diameter of tungsten wire |
| [S] | Area Matrix |
| h_c | Convective heat transfer coefficient |
| K_w | Thermal conductivity of air at surface of heated object |

| | |
|-----------------------|--|
| T_w | Surface temperature of wire |
| T | Ambient Temperature |
| $n(x,y)$ | Refractive index of heated air |
| $n_o(x,y)$ | Refractive index of ambient air |
| u | Molar mass of air |
| P | Atmospheric pressure |
| K | Gladstone-Dale Constant |
| R | Universal gas constant |
| $L \times W \times H$ | Length \times Width \times Height of heat sink |
| h | Thickness of base of heat sink |
| S | Channel width of heat sink |
| b | Thickness of heat sink |
| $Q(x)$ | Convective heat flux |
| $2t$ | Detector translation |
| l_M | Fringe spacing of modified grid |
| l_r | Fringe spacing of reference grid |
| Δh | Moiré contour interval |
| θ | Tilt in object illumination beam |
| β | Initial object illumination angle |

| | |
|-------|---|
| n_s | Refractive index of micro-lens material |
| h | Sag height of micro-lens |
| D | Diameter of micro-lens |
| ROC | Radius of curvature of micro-lens |
| J | Fringe spacing of sheared interferogram |